Thermal Lens Spectroscopy in Cryogenic Solutions: Analysis and Comparison of Intensities in CH_4-N_2 and CH_4-Ar Liquid Solutions

Alfredo Lopez-Calvo and Carlos E. Manzanares*

Department of Chemistry & Biochemistry, Baylor University, 101 Bagby Avenue, Baylor Sciences Building E-216, Waco, Texas 76798

Received: May 22, 2006; In Final Form: July 13, 2006

The C−H ($\Delta v = 6$) absorption spectrum of methane has been obtained in liquid nitrogen and argon solutions using thermal lens spectroscopy. Mathematical models for continuous and periodic excitation were used to describe the concentration dependence of thermal lens intensities. Better fitting of the experimental results was accomplished by taking into account the periodic nature of the excitation. Comparison of thermal lens intensities in nitrogen and argon allowed calculation of relative enhancement factors. In dilute solutions, the intensity in liquid nitrogen was 1.39 ± 0.08 times higher than that in argon. The literature estimation of this ratio is 1.49 ± 0.61. In contrast to the estimated value, our result confidently shows actual variation in enhancement factors. This article not only shows the applicability of thermal lensing to cryosamples but also demonstrates that accurate measurements at low temperature are possible.

1. Introduction

The thermal lens effect is commonly described as a change in the optical path of a sample caused by absorption of laser radiation having a Gaussian intensity profile (TEM_{00}).[1] The sample is most strongly heated at the beam center where the intensity is greatest, and the resulting temperature distribution is accompanied by an analogous change in the refractive index. In most liquids, the temperature gradient of the refractive index is negative, and so, the thermooptical element is shaped as a negative lens. The effect is generally detected at far field as a larger spot size or lower beam intensity. Since its discovery by Gordon and collaborators in 1965,[2,3] many applications of the thermal lens effect in chemistry have been explored. Some of them include the study of photochemical reactions,[4] the determination of energy-transfer rates,[5] and the measurement of thermal diffusivity.[6] Because of the intrinsic high sensitivity of photothermal techniques, the thermal lens effect has also found extensive applications in analytical chemistry[7,8] and the spectroscopy of weak molecular transitions.[9−11]

Vibrational overtones are a representative example of weak absorptions studied with thermal lens spectroscopy. The first report in this field was carried out by Swofford and coworkers[9,10] in 1976. They recorded overtone ($\Delta v = 5-7$) absorptions of C−H and O−H bonds in a variety of samples at room temperature.[12−14] Recently, Manzanares[15] reported the application of thermal lens spectroscopy to cryogenic samples, measuring the C−H ($\Delta v = 6$) overtone transition of liquid methane and methane−argon solutions. Previously, photoacoustic spectroscopy had been used to study these transitions in liquid methane[16,17] and ethylene.[18] Because thermal lensing allows analysis of dilute solutions, the advantages of liquefied rare gases as solvents can be fully exploited. High transparency in a broad spectral range, minimal perturbations of degrees of freedom, and optical homogeneity are always desirable solvent qualities in vibrational spectroscopy.[19]

The thermal lens effect has been described theoretically for a variety of experimental conditions. Whether the laser excitation is pulsed or continuous, the pump−probe geometry is collinear or transverse, and the sample is stationary or flowing, theoretical models have been developed to account for the experimental observations.[20,21] In every case, the intensity of the thermal lens is proportional to the sample absorbance, the excitation power (P), and the thermooptical properties of the solvent. Specifically, the thermal conductivity (k) and the temperature gradient of the refractive index (dn/dT) dictate the solvent effect. Comparison of thermal lens intensities in different media usually requires computation of enhancement factors.[22] This parameter is defined as

$$E = X\frac{1}{k}\left|\left(\frac{dn}{dT}\right)\right|\frac{Y_H P}{\lambda} \qquad (1)$$

where X is a factor that depends on the laser configuration, Y_H is the heat yield, and λ is the excitation wavelength. In theory, the enhancement factor represents the gain in analytical sensitivity with respect to absorption spectrophotometry.

The dual-beam technique was used in the present work to obtain the C−H ($\Delta v = 6$) overtone spectrum of methane−nitrogen and methane−argon mixtures. Using two simple theoretical models, the concentration dependence of thermal lens intensities was investigated. In addition, quantitation of the solvent effect between liquid nitrogen and argon was carried out. The analysis illustrates accurate application of the technique to cryogenic solutions.

2. Experimental Section

2.1. Thermal Lens Spectrometer. The experimental setup is depicted in Figure 1. The excitation laser was a continuous-wave dye laser (Coherent CR-599) pumped by an argon ion laser (Spectra Physics Stabilite 2017) tuned at 514 nm. The output power of the argon laser was 2.8 W, and the peak power of the dye laser was 500 mW. The dye laser was scanned in

* Corresponding author. E-mail: Carlos_Manzanares@baylor.edu.

10.1021/jp0631275 CCC: $33.50
Published on Web 08/17/2006

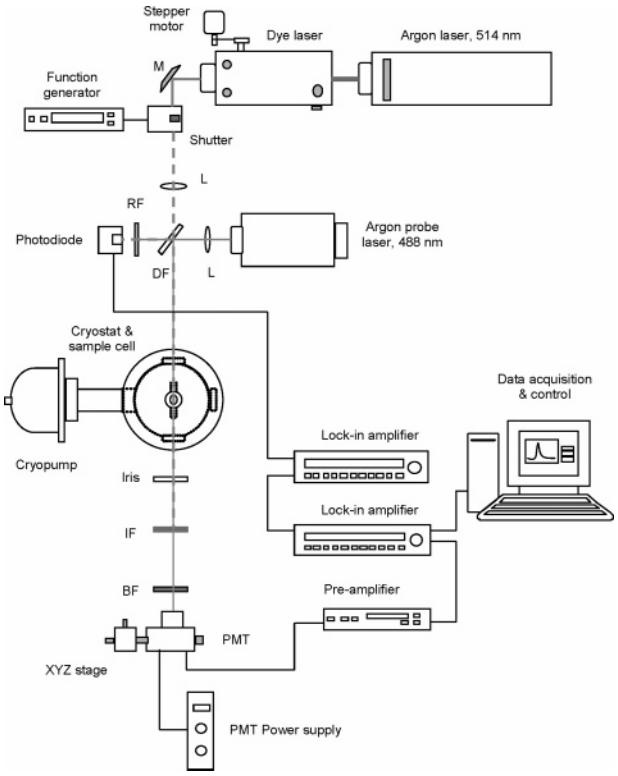

Figure 1. Experimental setup of the thermal lens spectrometer. Key: M, mirror; L, focusing lens; RF, red glass filter; DF, dichroic filter; IF, interference filter; BF, blue glass filter; PMT, photomultiplier tube.

the range of the laser dye (Kiton red) from 603 to 660 nm. The excitation beam was modulated by means of a low-frequency optical shutter (Electro-Optical Products Corp. CH-60), operated with a function generator (SRS DS345) at 5.0 Hz or lower frequencies depending on the application. Wavelength tuning of the dye laser (1 cm^{-1}) was carried out with a stepper motor, remotely controlled by a computer and LabView software. A second argon ion laser was used as a probe beam. The wavelength of the probe was 488 nm, and the output power was 6 mW. The excitation and probe beams were overlapped with a blue dichroic filter and propagated collinearly through the sample cell inside a cryostat. A photodiode was used to monitor the excitation beam power before the cryostat chamber. The excitation beam was focused at the sample cell; the spot radius and confocal distance were 0.030 and 51 cm, respectively. The probe beam was made larger than the excitation beam by a diverging lens. The spot radius of the probe beam at the cell was 0.091 cm, and the confocal distance was 0.87 cm. After emerging from the cryostat chamber, the beams passed through an iris placed in their path to spatially select the center of the probe beam. Next, an interference filter blocked the excitation beam and transmitted the probe beam. To eliminate any residual transmission of the excitation beam, a blue glass filter was placed after the interference filter. The intensity of the probe beam was measured with a photomultiplier tube (GCA McPherson EU-701-93). A 20-μm-diameter pinhole mounted on an XYZ stage allowed precise location of the thermal lens signal (TLS), as well as maximization of the intensity. Single-phase lock-in amplifiers (Ithaco 3962A) were used to monitor the thermal lens signal and the power output of the excitation laser. A normalized signal was obtained by dividing the outputs of the two lock-in amplifiers. The ratio was acquired, processed, and plotted by a LabView graphical interface.

The vacuum chamber was a cylindrical aluminum piece, measuring 18 cm in length and 22 cm in external diameter. The unit was equipped with three symmetrically placed quartz windows. Each window was 5.0 cm in diameter and 0.5 cm thick. Thermal isolation was achieved by having the chamber evacuated at pressures below 10^{-7} Torr, by means of a high-vacuum cryopump (CTI-Cryogenics, Helix Cryo-Torr 8F). The sample cell was located inside the vacuum chamber, connected to the cold head of the cryostat (International Cryogenics, model 31-4000). The cell was a copper (OFHC) cylinder 2.5 cm in external diameter, 1.2 cm in internal diameter, and 10 cm in length. Sapphire windows were mounted at each end of the cell. The windows were 0.2 cm thick and 2.0 cm in diameter. The birefringence of the sapphire windows was tested by passing a laser beam through the windows at different orientations with respect to each other. There was no significant change in the power of the passing beam. The cell−window interface was sealed with indium O-rings, and the windows were fastened to the cell with flat circular flanges. Sample admission was achieved through two sets of stainless steel tubing connected to an external gas handling system. The tubing was 1.6 mm in diameter and 30 cm in length. The cell temperature was controlled by a Scientific Instruments SI-9700 unit with the following specifications: accuracy, $\pm$87 mK; resolution, 1 mK below 100 K; and controllability, $\pm$27mK. The temperature was measured by two silicon diode sensors (model SI-410), one attached to the cell and the other attached to the cryostat head. Temperature readout was provided by the same controller.

2.2. FT-IR Spectrometer. Fourier transform infrared (FT-IR) spectra of cryogenic solutions were recorded with a Nexus 670 spectrometer from Thermo Nicolet. The cryostat was a model LT-3-110 apparatus from APD Cryogenics. Rough vacuuming of the system was carried out by a mechanical pump, and high vacuum ($<10^{-4}$ Torr) was achieved with a diffusion pump. Silicon diode sensors in the cryostat head and the sample cell provided temperature readings displayed in an SI-9650 controller. Some specifications of this controller include an accuracy of $\pm$0.5 K, a resolution of 0.01 K, and a controllability of $\pm$0.02 K. The vacuum chamber was a cylindrical aluminum unit 18.5 cm in length and 11.5 cm in external diameter. Four quartz windows were symmetrically placed on every side. Each window was 2.5 cm in diameter and 0.6 cm thick. The window−chamber interface was sealed with rubber O-rings, and the windows were fastened with flat circular flanges. The cell was a brass piece 3.8 cm in length, 3.1 cm in each height and width, and 1.2 cm in internal diameter. Quartz windows, 2.5 cm in diameter and 0.6 cm thick, were mounted at each end of the cell, and a third window was mounted on the side. The cell−window interface was sealed with indium O-rings, and the windows were fastened to the cell with square flanges. Sample admittance was achieved by a $^1/_8$-in. male Swagelok-to-NPT adapter installed on the side.

2.3. Sample Preparation. Mixtures were prepared by admitting suitable amounts of methane (Aldrich, 99.0%), argon (Matheson, 99.9995%), and nitrogen (Matheson, 99.999%) into a 250-mL customized lecture bottle. In general, the amount of methane was estimated from pressure readings, whereas the amount of solvent gas was measured using a flowmeter. The lecture bottle was cooled with liquid nitrogen to admit the large amount of solvent. The molar concentration of methane was estimated as a ratio of pressures. A more accurate value was determined with a calibration curve of the IR absorption at 3086 cm^{-1}. Mixtures were prepared in a 10-cm glass cell having 3.8-cm sodium chloride windows, where exact amounts of gas were

admitted using a digital manometer (MKS 122AA) with 0.01-Torr precision. By measuring the absorbance of the samples at the same pressure and temperature as the calibration mixtures, accurate concentrations were obtained.

3. Results

C−H ($\Delta v = 6$) overtone spectra of methane dissolved in liquid nitrogen and argon were recorded using thermal lens spectroscopy. Application of this technique to methane−argon solutions was previously reported by our research group.[15] In the present study, both concentration and solvent dependency of the thermal lens signal was investigated. Mixtures were prepared in a wide concentration range, extending from pure methane to 0.3% mole fraction, and their thermal lens intensity was measured at 16090 cm^{-1} (band peak). The excitation power was 1.9 mW, and the chopping frequency was 5.0 Hz. Figure 2 shows the corresponding series of spectra for nitrogen (top) and argon (bottom) solutions. The spectral band extends from 609.8 nm (16400 cm^{-1}) to 632.9 nm (15800 cm^{-1}), and deconvolution yields two components assigned as the main overtone transition ($5\nu_1 + \nu_3$) and the combination band ($4\nu_1 + \nu_3 + 2\nu_4$). For CH_4(0.34%)−N_2 and CH_4(0.35%)−Ar, the positions of the main peak are 16089 and 16077 cm^{-1}, and the bandwidths (fwhm) are 167 and 152 cm^{-1}, respectively. Because of the poor signal-to-noise ratio at 1.9 mW, spectra of these dilute solutions were acquired at 47 mW and linearly scaled to match the other traces. Band intensities of the 0.3% and 4% mixtures are compared in Figure 3. The molar concentrations of these solutions are 0.094 and 1.48 mol/L in nitrogen and 0.12 and 1.28 mol/L in argon. The intensities are higher in nitrogen even though the molarity of the dilute solution is lower than that in argon. This result clearly demonstrates greater signal enhancement.

Figure 4 shows C−H ($\Delta v = 5$) overtone spectra of methane−argon solutions at 87 K. These bands were recorded with an FT spectrometer. The absorbance of the fifth overtone was estimated from the fourth overtone value and the reported[16] fifth-to-fourth intensity ratio in pure methane. Results show that absorbance and molar concentration do not correlate linearly for all mixtures. In Figure 5, the absorbance results for argon (full circles) and nitrogen (open circles) solutions are plotted together for comparison. The unit of molar concentration was chosen to account for density variations. Notably, there is no apparent difference in the absorbances of nitrogen and argon solutions having the same molarity.

4. Discussion

4.1. Overtone Absorbance in Finite Mixtures. In a previous report,[15] the overtone absorbance of methane−argon solutions was assumed to be proportional to solute mole fraction. According to Beer's Law, such behavior is expected for dilute solutions; however, deviations are generally observed for high concentrations. Assuming the absence of instrumental effects, chemical associations and molecular scattering associated with high absorbance are often responsible for nonlinearity. Because the intensity of vibrational overtones is so low, deviations from linearity must be caused by increased solute−solute interactions.[23] Inspection of Figure 5 reveals that concentrated methane solutions exhibit lower than expected absorption coefficients. Moreover, no difference is detected in either nitrogen or argon solutions, which suggests similar intermolecular interactions. The latter result allows direct comparison of TLS intensities between these solvents.

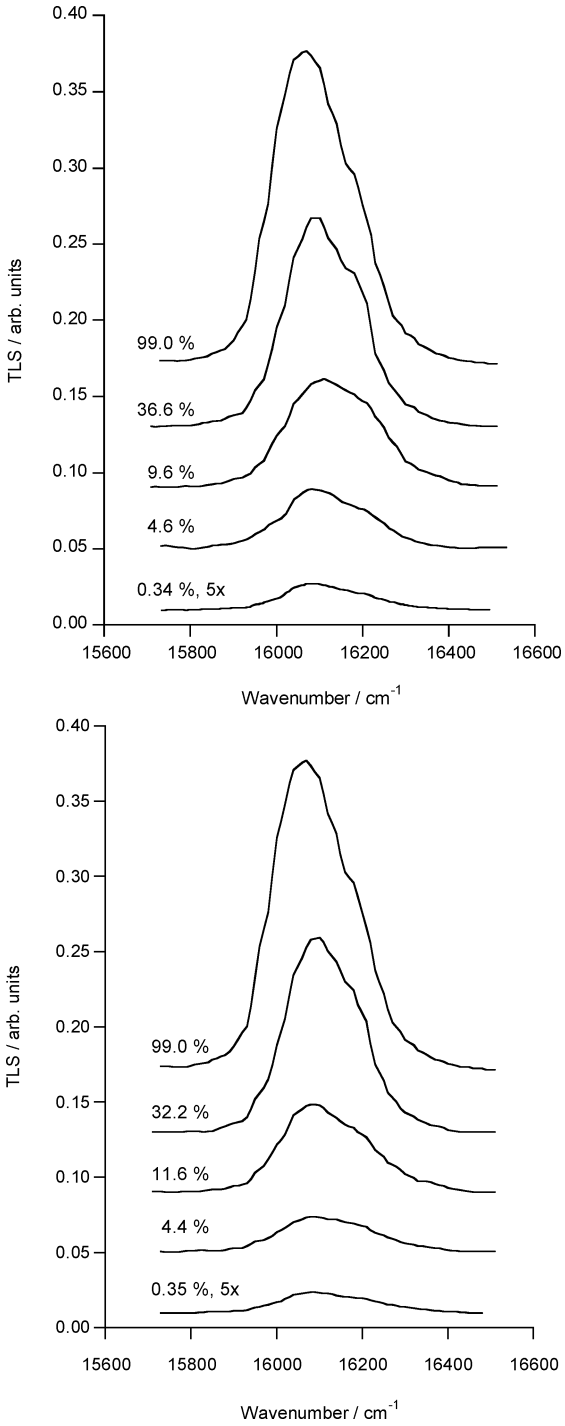

Figure 2. C−H ($\Delta v = 6$) TLS spectra of methane−nitrogen (top) and methane−argon (bottom) solutions at 85 K. Excitation power of 1.9 mW.

4.2. Concentration Dependence of Thermal Lens Intensities. Our analysis of concentration dependence is based on comparison between experimental results and simulated data from theoretical models. In addition to the continuous-excitation model,[22] a periodic-excitation approach[24] was included in the analysis to closely reflect our experimental conditions. Equation 2 presents the first case, a simple expression for signal intensity when continuous excitation is used

$$S_{cw}(t) = \frac{I(0) - I(t)}{I(t)} = (\alpha l)\left[-\frac{1}{k}\left(\frac{dn}{dT}\right)_P\right]\left(\frac{Z_1}{\pi w^2}\right)\left(\frac{1}{1 + t_c/2t}\right)(PY_H) \quad (2)$$

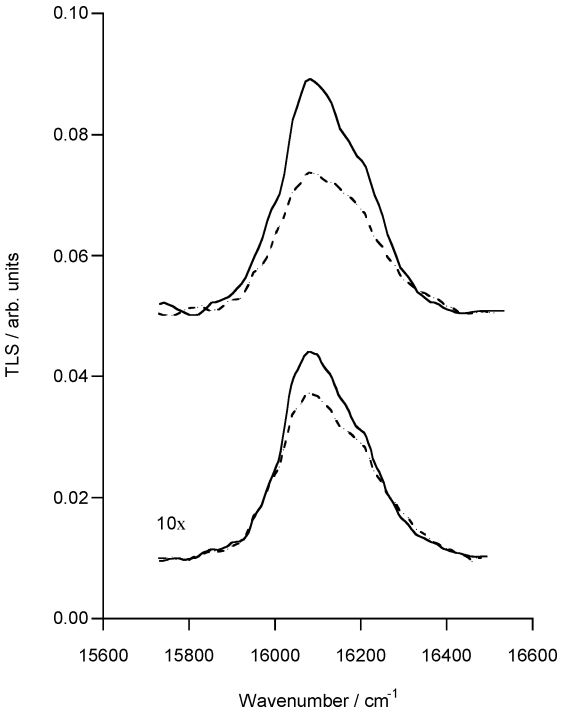

Figure 3. Comparison of band intensities between nitrogen (full line) and argon solutions (dashed line). The concentrations in nitrogen are 1.48 mol/L (4.6%) and 0.094 mol/L (0.34%), and those in argon are 1.28 mol/L (4.4%) and 0.12 mol/L (0.35%).

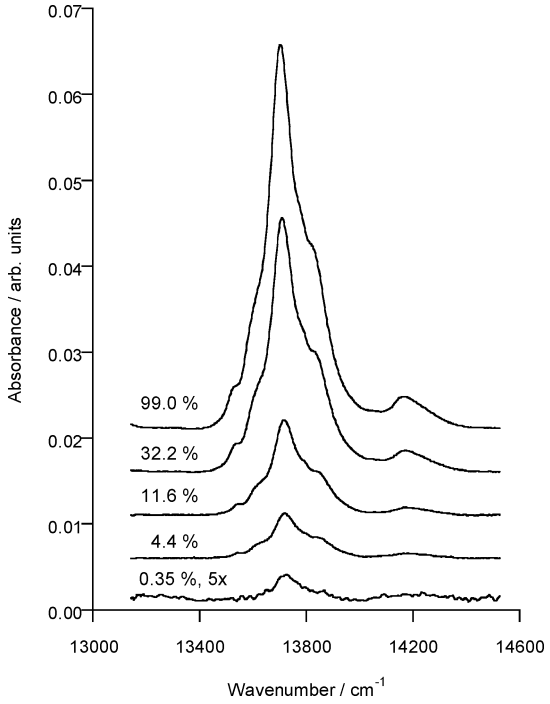

Figure 4. C−H ($\Delta\upsilon = 5$) absorption spectra of methane−argon solutions at 87 K. Spectra obtained with an FT spectrometer. Optical path length of 3.8 cm.

where $I(0)$ and $I(t)$ are the initial and final probe beam intensities, respectively. The first term in parentheses is the sample absorbance, where α is the absorption coefficient and l is the optical path length. The second term contains thermooptical properties of the solvent, specifically, the thermal conductivity (k) and the temperature gradient of the refractive index (dn/dT). The third term depends on the geometric arrangement of

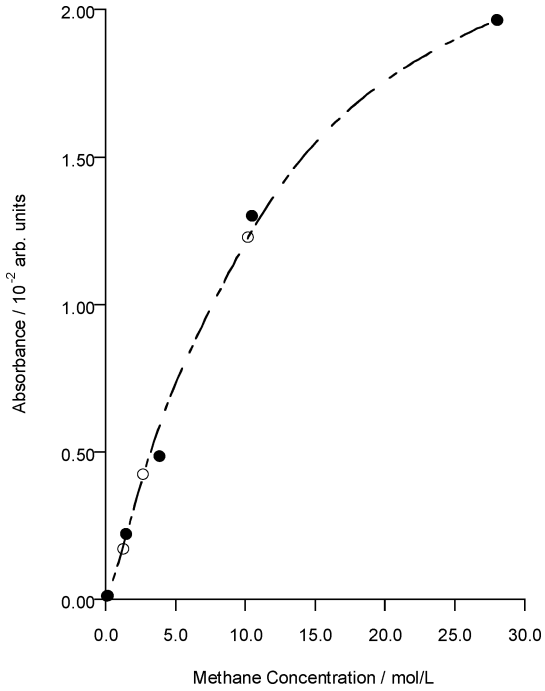

Figure 5. Estimated C−H ($\Delta\upsilon = 6$) absorption of methane−nitrogen (○) and methane−argon (●) solutions at 87 K. Optical path length of 10 cm. The absorbance of the fourth overtone was measured with an FT spectrometer.

the setup; Z_1 is the distance between the cell and the focal point of the probe beam, and w is the excitation beam spot radius. The fourth term contains the thermal lens relaxation constant ($t_c = w^2\rho C_p/4k$), where ρ is the medium density and C_p the heat capacity. The last term in parentheses is the laser power transformed into thermal energy; P is the laser power, and Y_H is the heat yield.

When periodic excitation is used, the contribution from previous chopping cycles should be taken into account in the simulation of the thermal lens signal. In general, incomplete TLS decay between chopping cycles results in lower intensities than predicted by the continuous-excitation model. Swofford[24] realized the necessity of including this effect in the analytical description of the thermal lens and derived the corresponding equation. The signal intensity is computed by

$$S_{CE}(t_m) = \frac{I(0;m) - I(\tau;m)}{I(0;0)} = 2Z_1\left[\frac{1}{F(0;m)} - \frac{1}{F(\tau;m)}\right] \quad (3)$$

$$\frac{1}{F(\tau_m;m)} = \frac{1}{k}\left(\frac{dn}{dT}\right)\left(\frac{P\alpha l}{\pi w^2}\right)\left\{\frac{1}{1+\frac{t_c}{2t}} + \sum_{i=1}^{m-1}\left[\frac{1}{1+\frac{2(A_i+\tau)}{t_c}} - \frac{1}{1+\frac{2(A_i+\tau)}{t_c}}\right]\right\} \quad (4)$$

$$A_i = t_m + \tau' + (i-1)(\tau+\tau') \quad (5)$$

where τ and τ' are the chopper "on" and "off" times, respectively; F is the focal length of the thermal lens; t_m denotes the time after the beginning of the mth chopper cycle, with $0 \le t_m \le \tau$; and all other variables have been defined previously.

TABLE 1: Thermophysical Properties[a] of Liquid Nitrogen and Argon at 85 K and Liquid Methane at 92 K

property	symbol	units	nitrogen	argon	methane
refractive index	n	−	1.1928	1.2238	1.2935
temperature gradient of the index of refraction	dn/dT	K^{-1}	−0.0012[b]	−0.0008[b]	−0.0010
molar density	r	mol/cm^3	27.49	35.28	28.03
thermal conductivity	k	W/(m K)	0.130	0.129	0.210
thermal expansion coefficient	b	K^{-1}	0.0062	0.0044	0.0031
heat capacity	C_p	J/(mol K)	58.57	44.57	54.10

[a] From refs 25, 30−38. [b] Average from several values; see Table 2.

TABLE 2: Temperature Gradient of the Refractive Index [dn/dT (K^{-1})] for Liquid Nitrogen and Argon at 85 K

source	nitrogen	argon
CRC[25]	−0.0013	−0.0004
Johns[34]	−0.0010 ± 0.0002	
Ely[35]	−0.0013 ± 0.0001	
Sinnock[30]		−0.0010 ± 0.0005
Amey[36]		−0.0007 ± 0.0003
Abbis[37]		−0.0010 ± 0.0001
Jones[38]		−0.0011 ± 0.0002
average	−0.0012 ± 0.0002	−0.0008 ± 0.0003

TLS intensities can be calculated with eq 3 once the initial ($t_m = 0$) and final ($t_m = \tau$) focal lengths have been evaluated. In the present work, the summation in eq 4 was carried out for $i = 50$ cycles.

For samples analyzed under the same experimental conditions, thermal lens intensities mainly depend on the sample absorbance and the thermooptical properties of the medium. In dilute solutions, the solvent properties can be used to evaluate eqs 2 and 3; however, finite mixtures require computation of these quantities based on their concentration. Assuming that methane−argon and methane−nitrogen systems form ideal solutions, mixture properties can be estimated using linear equations of the type $M = M_1 + (M_2 - M_1)x_2$, where M is any given property, x is the mole fraction, and the subindex indicates pure solvent (1) or pure solute (2).[25,26] The temperature gradient of the refractive index can be calculated using the Lorentz−Lorenz equation,[27,28] taking the derivative of the explicit expression reported by Heller.[15,29] A summary of the thermooptical properties[30−33] required by the simulations is presented in Table 1. Because the uncertainty in the temperature gradient of the refractive index for liquid nitrogen and argon is high, an average from different sources[25,30,34−38] was used. Table 2 shows individual and averaged results for both solvents. In every case, the gradient was computed from refractive index values measured at different temperatures. Whenever only the dielectric constant (ϵ) was reported, the refractive index (n) was first calculated using $n = \epsilon^{1/2}$, a valid approximation for nonpolar solvents.[39]

The concentration dependence of the thermal lens signal is shown in Figure 6. The graphs at the top and bottom correspond to nitrogen and argon solutions, respectively. Normalization by the highest intensity (pure methane) was carried out for comparison purposes. Experimental points represent signals relative to the initial probe intensity, which are compared to estimations from the periodic-excitation model (dashed line). Calculations from the continuous-excitation model (solid line) are also included, although no direct comparison with our results is possible because they are relative to the final probe intensity. A different axis was assigned to each quantity to point out the difference. Generally, these signals have similar magnitudes because the change in the probe beam intensity is small. Inspection of Figure 6 reveals the analogy in the concentration trends. In both solvents, close fitting of our observations is accomplished by the periodic-excitation approach. This result is attributed to precise measurement of TLS intensities and accurate knowledge of relative absorbances. In the case of the continuous-wave (cw) model, no fitting improvement was observed when plotting the corresponding experimental points. As a result, we concluded that taking into account the periodic nature of the excitation provides a better description of the concentration trend. A comparison between the nitrogen and argon plots reveals slight variations in the shapes of the curves. This nuance is attributed to intrinsic variations in the thermooptical properties of the solvents.

4.3. Solvent Effect on Thermal Lens Intensities. The solvent effect on the intensity of the thermal lens is shown in Figure 7. All samples were analyzed with the same excitation power. Experimental points are connected by smooth lines, and molarity is chosen again as the concentration unit to account for density variations. Clearly, the intensities in nitrogen are slightly higher than those in argon. The error bars represent the standard deviation of at least 10 measurements. As previously discussed, the absorption coefficients of methane−argon and methane−nitrogen solutions having the same molarity are equivalent. In addition, the relaxation time constants (t_c) of the solvents are practically identical. Consequently, the intensity shift observed in Figure 7 must be caused by thermooptical properties. Recalling eqs 2 and 3, variations in the thermal conductivity (k) and the temperature gradient of the refractive index (dn/dT) are responsible. The intensity shift is mainly attributed to the latter, because the solvents have similar thermal conductivities (see Table 1). For any two solutions that share similar relaxation time constants, a relative solvent effect can be calculated with

$$\frac{\left[\frac{\Delta I(0,\tau;m)}{\alpha}\right]_{\text{nitrogen}}}{\left[\frac{\Delta I(0,\tau;m)}{\alpha}\right]_{\text{argon}}} = \frac{\left(\frac{1}{k}\frac{dn}{dT}\right)_{\text{nitrogen}}}{\left(\frac{1}{k}\frac{dn}{dT}\right)_{\text{argon}}} \qquad (6)$$

Normalization of the TLS intensities by the absorbance was carried out, and their ratio was taken for mixtures with similar concentration. Results are summarized in Table 3. A comparison of the t_c values between nitrogen and argon solutions is provided as a reference. The quantity calculated in eq 6 represents the ratio of enhancement factors between the mixtures. Accordingly, the result obtained with dilute solutions estimates the relative enhancement of the solvents. Using the information in Tables 1 and 2, the expected nitrogen-to-argon ratio is 1.49 ± 0.61. Even though the estimated value suggests greater enhancement in liquid nitrogen, confidence is undermined by its high uncertainty. In contrast, the experimental average result of 1.39 ± 0.08 clearly supports the observation. The estimated and experimental ratios have similar magnitudes, but only the low

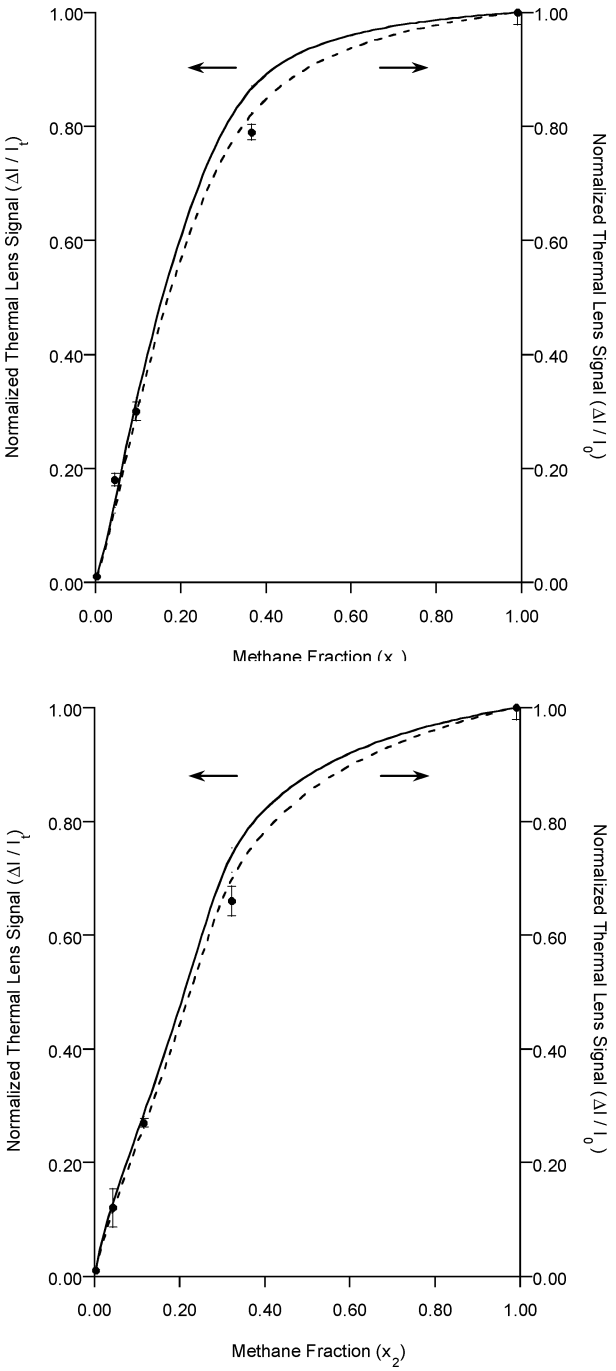

Figure 6. Concentration dependence of the thermal lens signal in methane−nitrogen (top) and methane−argon (bottom) solutions. Experimental points (●) are relative to the initial probe intensity. Results from the periodic-excitation model (dashed line) are plotted on the left axis, and results from the continuous-excitation model (solid line) are plotted on the right axis.

uncertainty in the latter indicates actual variation in the enhancement factors. Because different excitation powers were used with the dilute solutions, the enhancement ratio was also calculated from the slope of the power plots. Figure 8 shows not only the proportionality of the TLS intensities with power, but also the difference in enhancement factors between the solvents (slopes); the corresponding result is 1.44 ± 0.10. In the case of higher concentrations, lower solvent effects were obtained. As expected, the contribution of the solvent becomes smaller as the molar fraction of methane increases. An enhancement ratio of 1.17 ± 0.06 still remains for $CH_4(36.6\%)-N_2$ and $CH_4(32.2\%)-Ar$. Certainly, no solvent effect would be detected for higher concentrations because of the similarity in thermooptical properties.

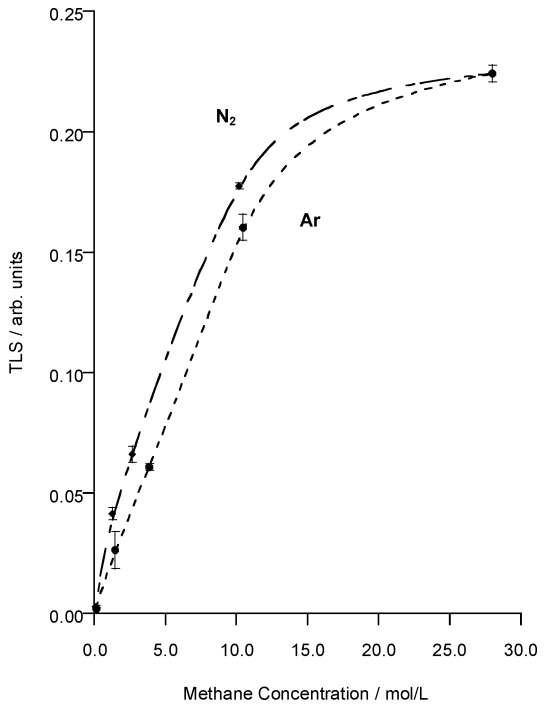

Figure 7. Comparison of TLS intensities between methane−nitrogen (◆) and methane−argon (●) solutions at 85 K.

TABLE 3: Experimental Ratio of Enhancement Factors between Methane−Nitrogen and Methane−Argon Solutions at 85 K

methane mole fraction (% in N_2/% in Ar)	ratio of relaxation time constants $(t_c)_{N2}/(t_c)_{Ar}$	excitation power (mW)	$(\Delta I/\alpha)_{N2}/(\Delta I/\alpha)_{Ar}$ (arb units)
0.34/0.35	1.01	8.0	1.42 ± 0.36
		15.0	1.40 ± 0.06
		27.0	1.38 ± 0.11
		38.0	1.30 ± 0.07
		47.0	1.49 ± 0.06
			1.39 ± 0.08[a]
			1.44 ± 0.10[b]
			1.49 ± 0.61[c]
4.6/4.4	1.01	1.9	2.05 ± 0.60
9.6/11.6	1.02	1.9	1.23 ± 0.07
36.6/32.2	0.99	1.9	1.17 ± 0.06

[a] Average. [b] Slope ratio. [c] Literature estimation.

Absolute enhancement factors of cryosolvents are generally high. Using the definition given in eq 1, the values for nitrogen and argon at 85 K are 9662 and 6491, respectively. A 500-nm excitation source operating at 1 W was used in the calculation. Results for common solvents at room temperature were reported by Bialkowski[22] using the same excitation parameters. Carbon tetrachloride showed the highest enhancement of 6220. In addition to favorable thermooptical properties, we speculate that signal enhancement in cryosolvents is also amplified by the heat yield (Y_H). Because monatomic gases do not have vibrational degrees of freedom, most of the energy transferred to the solvent contributes to increasing the temperature. Consequently, the density and refractive index suffer larger perturbations. A similar result is expected for condensed diatomic gases, such as hydrogen, oxygen, and nitrogen. The combined effect of favorable properties and high heat yield make cryosolvents

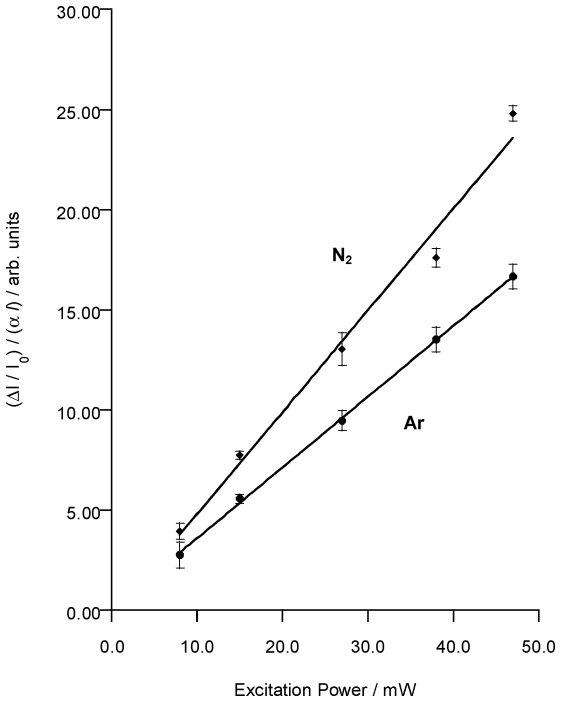

Figure 8. Ratio of thermal lens signal to sample absorbance for CH_4-(0.34%)−N_2 and CH_4(0.35%)−Ar solutions at different excitation powers.

particularly attractive for photothermal studies. As shown in this article, difficulties associated with working at low temperature can be overcome. Thus, increased motivation is anticipated regarding the application of thermal lensing to cryosolutions.

5. Conclusion

The C−H ($\Delta\upsilon = 6$) absorption spectrum of methane has been obtained in liquid nitrogen and argon solutions using thermal lens spectroscopy. No particular solvent effects on the bandwidth and location of TLS spectra were observed. The C−H ($\Delta\upsilon = 5$) absorption spectra of these mixtures were also recorded with an FT-IR spectrometer, revealing deviation from Beer's Law for high methane concentrations. Moreover, the analysis suggested that the absorption coefficients in the two solvents are equivalent. Comparison of thermal lens intensities against theoretical simulations indicates that similar trends with concentrations are followed; specifically, a better fitting is obtained with the periodic-excitation model. The solvent effect on thermal lens intensities was clearly observed. Nitrogen solutions showed slightly higher intensities than argon solutions having the same molar concentration of methane. This effect was mainly attributed to different values of the temperature gradient of the refractive index (dn/dT). In dilute solutions, the intensity in liquid nitrogen was 1.39 ± 0.08 times higher than that in argon. The literature estimation of this ratio is 1.49 ± 0.61. In contrast to the estimated value, our result confidently shows an actual difference in enhancement factors. The analysis presented in this article illustrates the applicability of thermal lensing to low temperatures and shows the possibility of carrying out accurate measurements in cryosolutions.

Acknowledgment. This work was supported by the Robert A. Welch Foundation under Grant AA-1173. This study was supported in part by funds from the Quantum Optics Initiative funded by the ONR, Texas A&M, and the Vice Provost for Research at Baylor University. Partial support from the Baylor University Research Committee is also acknowledged.

References and Notes

(1) Harris, J. M. Thermal Lens Effect. In *Analytical Applications of Lasers*; Piepmeier, E. H., Ed.; Chemical Analysis 87; Wiley & Sons: New York, 1986; pp 451−455.

(2) Leite, R. C.; Moore, R. S.; Whinnery, J. R. Low Absorption Measurements by Means of the Thermal Lens Effect Using a He−Ne Laser. *Appl. Phys. Lett.* **1964**, *5*, 141−143.

(3) Gordon, J. P.; Leite, C. C.; Moore, R. S.; Porto, P. S.; Whinnery, J. R. Long-Transient Effects in Lasers with Inserted Liquid Samples. *J. Appl. Phys.* **1965**, *36*, 3−8.

(4) Mladen, F.; Chieu, T. Thermal Lens Technique for Sensitive Kinetic Determination of Fast Chemical Reactions. Part II. Experiment. *Rev. Sci. Instrum.* **1991**, *62*, 2438−2442.

(5) Grabiner, F. R.; Siebert, D. R.; Flynn, G. W. Laser Induced Time-Dependent Thermal Lensing Studies of Vibrational Relaxation: Translational Cooling in CH_3F. *Chem. Phys. Lett.* **1972**, *17*, 189−193.

(6) Bindhu, C. V.; Harilal, S.; Nampoori, V.; Vallabhan, C. Thermal Diffusivity Measurements in Organic Liquids Using Transient Thermal Lens Calorimetry. *Opt. Eng.* **1998**, *37*, 2791−2794.

(7) Georges, J. Advantages and Limitations of Thermal Lens Spectrometry over Conventional Spectrophotometry for Absorbance Measurements. *Talanta* **1999**, *48*, 501−509.

(8) Navas, M.; Jimenez, A. Thermal Lens Spectrometry as Analytical Tool. *Crit. Rev. Anal. Chem.* **2003**, *33*, 77−88.

(9) Swofford, R.; Long, M.; Albrecht, A. C−H Vibrational States of Benzene, Naphthalene, and Anthracene in the Visible Region by Thermal Lensing Spectroscopy and the Local Mode Model. *J. Chem. Phys.* **1976**, *65*, 179−190.

(10) Swofford, R.; Long, M.; Albrecht, A. Thermal Lens Technique: A New Method of Absorption Spectroscopy. *Science* **1976**, *191*, 183−185.

(11) Hineman, M.; Rodriguez, R.; Wibler, J. Photothermal Lensing Spectroscopy of Supersonic Jet Expansions of Acetylene. *J. Chem. Phys.* **1988**, *89*, 2630−2634.

(12) Fang, H.; Swofford, R. Highly Excited Vibrational States of Molecules by Thermal Lensing Spectroscopy and Local Mode Model. II. Normal, Branched, and cyclo-Alkanes. *J. Chem. Phys.* **1980**, *73*, 2607−2617.

(13) Swofford, R.; Burberry, M.; Morrell, J.; Albrecht, A. C−H Vibrational States of Benzene-d_5 and Benzene-f_5 in the Visible Region by Thermal Lens Spectroscopy. A Test of the Local Mode Model. *J. Chem. Phys.* **1977**, *66*, 5245−5246.

(14) Swofford, R.; Long, M.; Burberry, M.; Albrecht, A. Free OH Overtone Absorption of Methanols in the Visible Region by Thermal Lensing Spectroscopy. *J. Chem. Phys.* **1977**, *66*, 664−668.

(15) Navea, J.; Lopez-Calvo, A.; Manzanares, C. Thermal Lens Spectroscopy in Liquid Argon Solutions: ($\Delta\upsilon = 6$) CH Vibrational Overtone Absorption of Methane. *J. Phys. Chem. A* **2006**, *110*, 1594−1599.

(16) Patel, C.; Nelson, E.; Kerl, R. Opto-acoustic Study of Weak Optical Absorption on Liquid Methane. *Nature* **1980**, *286*, 368−370.

(17) Blunt, V.; Cedeño, D.; Manzanares, C. Vibrational Overtone Spectroscopy of Methane in Liquid Argon Solutions. *Mol. Phys.* **1997**, *91*, 3−17.

(18) Nelson, E.; Patel, C. Visible Absorption Spectrum of Liquid Ethylene. *Proc. Natl. Acad. Sci.* **1981**, *78*, 702−705.

(19) Bulanin, M. Liquefied Gases as Solvents for Vibrational Spectroscopy. In *Handbook of Vibrational Spectroscopy*; Chalmers, J., Griffiths, P., Eds.; John Wiley & Sons: New York, 2001; pp 1329−1341.

(20) Gupta, R. *The Theory of Photothermal Effect in Fluids. Photothermal Investigations of Solids and Fluids*; Academic Press: New York, 1989; pp 81−126.

(21) He, Q.; Vyas, R.; Gupta, R. Photothermal Lensing Detection: Theory and Experiment. *Appl. Opt.* **1997**, *36*, 7046−7058.

(22) Bialkowski, S. *Photothermal Spectroscopy Methods for Chemical Analysis*; Chemical Analysis 134; Wiley & Sons: New York, 1996.

(23) Griffiths, P. Introduction to Vibrational Spectroscopy. In *Handbook of Vibrational Spectroscopy*; Chalmers, J., Griffiths, P., Eds.; John Wiley & Sons: New York, 2001; pp 34−57, 2225.

(24) Swofford, R.; Morrell, J. Analysis of the Repetitively Pulsed Dual-beam Thermo-optical Absorption Spectrometer. *J. Appl. Phys.* **1978**, *49*, 3667−3674.

(25) *CRC Handbook of Chemistry and Physics*, 84th ed.; Lide, D., Ed.; CRC Press: Boca Raton, FL, 2004−2005; pp 6/155−6/157.

(26) Heyes, D. Molecular Dynamics Simulations of Liquid Binary Mixtures: Partial Properties of Mixing and Transport Coefficients. *J. Chem. Phys.* **1992**, *96*, 2217−2227.

(27) Lorentz, H. Über die Beziehungzwischen der Fortpflanzungsgeschwindigkeit des Lichtes der Körperdichte. *Ann. Phys.* **1880**, *9*, 641−665.

(28) Lorenz, L. Über die Refractionsconstante. *Ann. Phys.* **1881**, *11*, 70−103.

(29) Heller, W. Remarks on Refractive Index Mixture Rules. *J. Phys. Chem.* **1965**, *69*, 1123−1129.

(30) Sinnock, A. Refractive Indices of Condensed Rare Gases, Argon, Krypton, and Xenon. *J. Phys. C: Solid State Phys.* **1980**, *13*, 2375−2391.

(31) Lemmon, E.; McLinden, M.; Friend, D. Thermo-physical Properties of Fluid Systems. In *NIST Chemistry WebBook*; NIST Standard Reference Database Number 69; Linstrom, P., Mallard, W., Eds.; National Institute of Standards and Technology: Gaithersburg, MD, 2005; 20899 (http://webbook.nist.gov).

(32) Badoz, J.; Le Liboux, M.; Nahoum, R.; Israel, G.; Raulin, F.; Torre, J. A Sensitive Cryogenic Refractometer. Application to the Refractive Index Determination of Pure or Mixed Liquid Methane, Ethane, and Nitrogen. *Rev. Sci. Instrum.* **1992**, *63*, 2967−2973.

(33) Younglove, B.; Ely, J. Thermo-physical Properties of Fluids. II. Methane, Ethane, Propane, Isobutane and Normal Butane. *J. Phys. Chem. Ref. Data* **1987**, *16*, 577−761.

(34) Johns, H.; Wilhelm, J. The Refractive Indices of Liquid Oxygen, Nitrogen, and Hydrogen. *Can. J. Res. A* **1937**, *15*, 101−108.

(35) Ely, J.; Straty, G. Dielectric Constants and Molar Polarizabilities of Saturated and Compressed Fluid Nitrogen. *J. Chem. Phys.* **1974**, *61*, 1480−1485.

(36) Amey, R.; Cole, R. Dielectric Constants of Liquefied Noble Gases and Methane. *J. Chem. Phys.* **1964**, *40*, 146−148.

(37) Abbiss, C.; Knobler, C.; Teague, R.; Pings, C. Refractive Index and Lorentz−Lorenz Functions for Saturated Argon, Methane and Carbon Tetrafluoride. *J. Chem. Phys.* **1965**, *42*, 4145−4148.

(38) Jones, G.; Smith, B. The Refractive Indices of Liquid and Solid Argon. *Philos. Mag.* **1960**, *5*, 355−358.

(39) . Bayliss, N.; Cole, A.; Little, L. Solvent Effects in Infrared Spectra: C═O, C−H, and C−C Vibrations. *Aust. J. Chem*. **1955**, *8*, 26−38.